Peer-reviewed version available at *Micromachines* **2019**, *10*, 797; doi:10.3390/mi10120797

Article

Simulation of an Adaptive Fluid-Membrane Piezoelectric Lens

Hitesh Gowda Bettaswamy Gowda [1], and Ulrike Wallrabe [1,*]

[1] Affiliation 1; Laboratory for Microactuators, Department of Microsystems Engineering - IMTEK, University of Freiburg, Georges-Köhler-Alle 102, Room 02-081, Freiburg Im Breisgau, Germany-79110.

* Correspondence: wallrabe@imtek.uni-freiburg.de; Tel.: +49 (0) 761 203-7580

Abstract: In this paper, we present a finite element simulation of an adaptive piezoelectric fluid-membrane lens modelled in COMSOL Multiphysics®. The simulation couples the piezoelectric effect with the fluid dynamics to model the interaction between the piezoelectric forces and the fluid forces. Also, the simulation is extended to model the thermal expansion of the fluid. Finally, we compare the simulation and experimental results of the adaptive lens refractive power at different actuation levels and temperatures.

Keywords: Adaptive lens; Piezoelectric devices; Fluid-structure interaction; Moving mesh; Thermal expansion.

1. Introduction

The expression adaptive optics was initially termed for the technology used in telescopes to deform the mirrors for phase correction of the incoming light [1]. Soon, adaptive optics was implemented in microscopes [2], optical communication systems [3], and optical imaging systems [4]. In conventional imaging systems, the lenses are mechanically moved to focus an image, whereas, with the adaptive optics lens, the surface curvature of the lens is changed to focus an image. The focus tunable lens, or also known as the adaptive lens, uses different actuation principles to change the curvature of a deformable surface, thereby changing the focus (refractive power) of the lens. One such adaptive lens utilizing a piezoelectric actuation principle to deform a fluid-membrane interface [5] was developed in the Laboratory for Microactuators, Department of Microsystems Engineering-IMTEK, University of Freiburg, Germany.

The adaptive lens consists of a piezoelectric actuator, a fluid chamber, and a transparent flexible membrane, as shown in Figure 1a. The flexible membrane bounds the fluid chamber on one side, and hence any change in the fluid chamber pressure will deform the membrane. The circular design of the lens allows for a membrane deformation to form either a converging or a diverging lens, depending on the fluid chamber pressure. To change the fluid chamber pressure, the adaptive lens utilizes the inverse piezoelectric property of the actuator [6], which corresponds to the deformation of the piezo material under an applied electric field. With the applied electric field (voltage), the integrated piezoelectric actuator will deform the fluid chamber and change the fluid chamber pressure. By changing the electric field direction and magnitude, the fluid pressure can be varied to positive or negative pressures. The refractive power of the lens, which is proportional to the membrane curvature, is hence dependent on the fluid chamber pressure. The simulation setup aims to model the interaction between the piezoelectric deformation and the change in fluid chamber pressure that result in a deformation of the flexible membrane. Also, the simulation setup is extended to model the further deformation of the membrane due to the thermal expansion of the fluid. In the COMSOL Multiphysics®, multiple physics modules such as the piezoelectric devices, the fluid-structure interaction, the heat transfer in solids, and the heat transfer in fluids are coupled explicitly to model the adaptive lens.

Preprints (www.preprints.org) | NOT PEER-REVIEWED | Posted: 21 October 2019 doi:10.20944/preprints201910.0244.v1

Peer-reviewed version available at Micromachines 2019, 10, 797; doi:10.3390/mi10120797

2. The Fluid-Membrane Piezoelectric Lens

The piezoelectric bi-morph actuator has a circular ring-shaped design with the two piezoelectric ceramic layers glued together in an anti-parallel polarization configuration. The fluid chamber and the flexible membrane are integrated with the actuator using micro-molding techniques to form an active lens chamber [5]. The active lens chamber is glued onto a PCB based substrate [7] and primed with an optical oil [7] (Figure 1a).

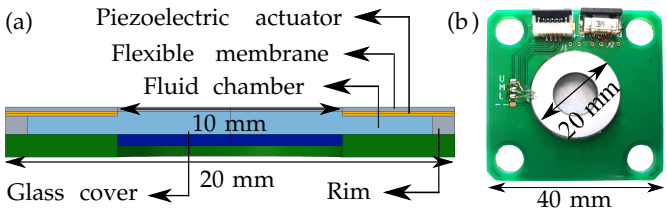

Figure 1. (a) 2D cut section of the adaptive lens to show the fluid chamber, flexible membrane, and the integrated actuator. (b) The adaptive fluid-membrane piezoelectric lens.

The manufactured adaptive lens with the actuator diameter of 20 mm at an aperture of 10 mm is shown in Figure 1b. Depending on the applied electric field / voltage direction, the piezoelectric actuator deforms the fluid chamber to produce positive or negative fluid chamber pressure. The positive pressure leads to a plano-convex lens (Figure 2a), and the negative pressure leads to a plano-concave lens (Figure 2b).

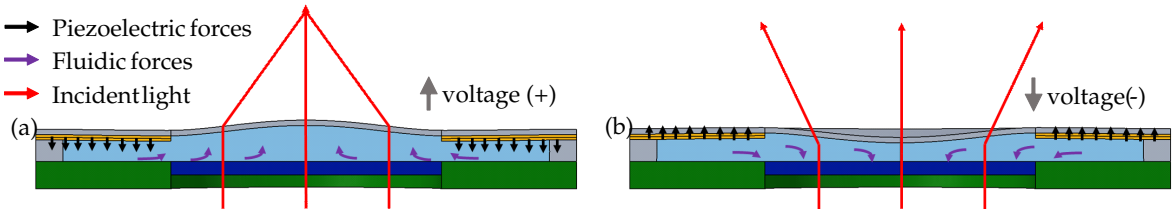

Figure 2. The 2D cross-section of the adaptive lens showing the piezoelectric forces and fluidic forces, which form either (a) plano-convex lens or (b) plano-concave lens depending on the applied voltage direction.

3. Multiphysics Simulation

To reduce the complexity of a 3*D* geometry and at the same time to decrease the computation time, a 2*D*-axisymmetric space dimension is chosen to model the adaptive lens (Figure 3). The materials used in the simulation are as mentioned in Table 1.

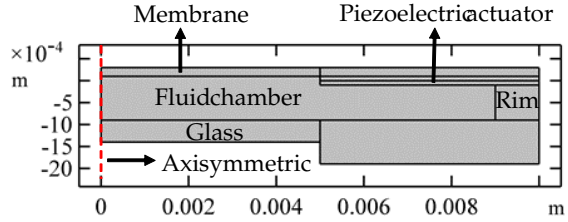

Figure 3. The 2D axisymmetric simulation model of the adaptive lens.

Peer-reviewed version available at Micromachines 2019, 10, 797; doi:10.3390/mi10120797

Table 1. The adaptive lens materials used in the simulation.

Component	Material
Piezoelectric actuator	Lead Zirconate Titanate (PZT-5H)
Flexible membrane, rim	PDMS - Polydimethylsiloxane
Fluid	Oil
Substrate	Glass (quartz)

3.1. Piezoelectric Devices

To model the inverse piezoelectric effect of the actuator, the piezoelectric devices module is used. The module couples the solid mechanics (Eq 1) and the electrostatics (Eq 2) physics to combine the electrical behavior and the mechanical behavior of the piezoelectric ceramics. The combined behavior is modelled through the coupled equations (Eq 3) and (Eq 4) in strain-charge form.

$$\rho \frac{\partial^2 u}{\partial^2 t} = \nabla \cdot S + F_v \tag{1}$$

$$E = -\nabla \cdot V \tag{2}$$

$$S = S_E T + d^T E \tag{3}$$

$$D = dT + \epsilon_o \epsilon_{rT} E \tag{4}$$

3.2. Fluid-Structure-Interaction

To model the fluid forces in the fluid chamber, the fluid-structure interaction (FSI) module is used. The FSI couples the solid mechanics (Eq 1) and the laminar flow (Eq 5) physics to model the fluid force interaction with the flexible membrane. The fluidic forces contribute to the deformation of the flexible membrane to an aspherical surface.

$$\rho \frac{\partial u_2}{\partial t} + \rho(u_2 \cdot \nabla)u_2 = \nabla \cdot [\rho I + \mu \nabla u_2] + F + \rho g \tag{5}$$

3.3. Heat Transfer in Fluids and Solids

Apart from the piezoelectric forces that contribute to the deformation of the membrane, the thermal expansion of the fluid at higher temperatures will as well cause the membrane deformation. Hence to model the fluid thermal expansion, heat transfer in fluids and heat transfer in solids (Eq 6) physics modules are used.

$$q = -k \nabla T \tag{6}$$

3.4. Moving Mesh

The adaptive lens working mechanism relies on the transfer of piezoelectric forces to the flexible membrane through the fluid pressure. In COMSOL Multiphysics®, the coupling of the piezoelectric effect and the fluid-structure interaction is not possible through a direct multiphysics feature. Hence, the moving mesh physics module is used to couple the piezoelectric forces with the fluid pressure and apply the resultant on the flexible membrane. The explicit coupling of piezoelectric and laminar physics is performed in a way such that the solid domain velocities (Eq 7) and (Eq 8) generated by the deformation of the piezoelectric actuator are applied as the mesh velocities on the walls of the fluid

Preprints (www.preprints.org) | NOT PEER-REVIEWED | Posted: 21 October 2019 doi:10.20944/preprints201910.0244.v1

Peer-reviewed version available at Micromachines 2019, 10, 797; doi:10.3390/mi10120797

chamber as shown in Figure 4c. The geometric domains with the free deformation mesh and with the fixed mesh are as shown in Figure 4a and Figure 4b, respectively.

$$V_r = solid \cdot u\_tR \tag{7}$$

$$V_z = solid \cdot u\_tZ \tag{8}$$

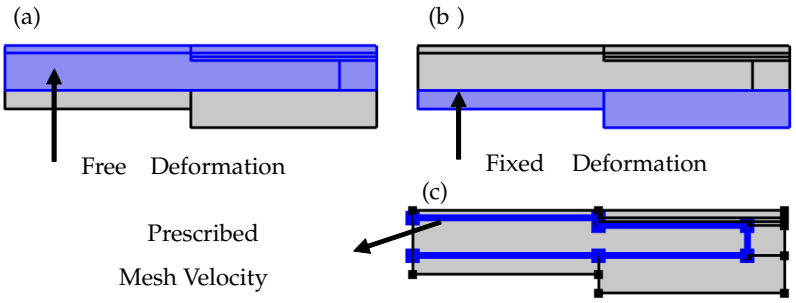

Figure 4. The domains specified in the Moving Mesh module to be (a) free mesh and (b) fixed mesh. (c) The solid domain velocity applied on the walls of the fluid chamber.

3.5. Boundary Condition

In the solid mechanics interface, the glass substrate is selected in the fixed constraint condition, as shown in Figure 6a. The piezo ceramic layers in the bi-morph actuator have an anti-parallel polarization configuration. To adapt for the polarization direction in the simulation, an additional base vector system is created with the base vector 'x3' set to -1 instead of default 1. The default base vector system is selected as the coordinate system for the piezo 1, and an additional base vector system is selected as the coordinate system for the piezo 2 (Figure 6b). In the heat transfer interface, all the boundaries are selected in the temperature constraint, to set the entire domain to required temperature (Figure 6c). In the laminar flow interface, the walls of the fluid chamber are selected with a no-slip boundary condition (Figure 6d). Since the fluid chamber is a closed domain, there is no inlet, outlet, or open boundary conditions.

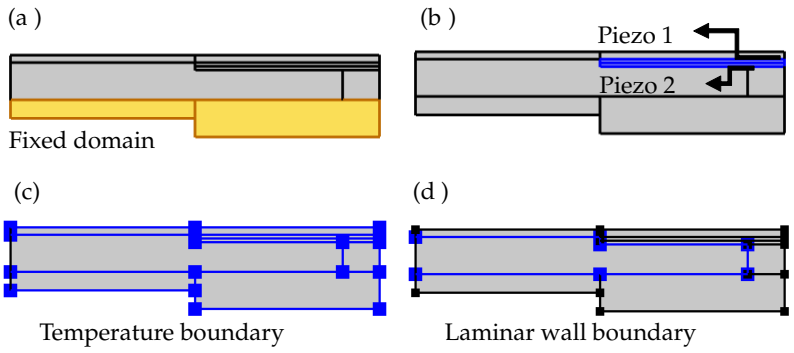

Figure 5. Boundary conditions of the domains in Solid Mechanics (a) and (b), Heat transfer in Solids and Fluid, and (c) Laminar Flow wall boundary.

3.6. Mesh

The simulation requires the walls of the fluid chamber to be finely meshed due to the change of the material state from solid to fluid. The edge feature with a fine mesh is used for the fluid wall and the physics controlled finer mesh is used for the rest geometry.

Preprints (www.preprints.org) | NOT PEER-REVIEWED | Posted: 21 October 2019 doi:10.20944/preprints201910.0244.v1

Peer-reviewed version available at Micromachines 2019, 10, 797; doi:10.3390/mi10120797

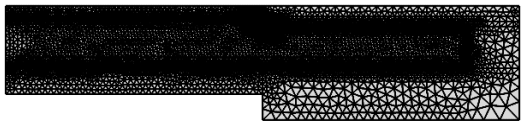

Figure 6. The meshing of the adaptive lens.

4. Results

The time dependent study was selected in the simulation as the velocities, which are used in the moving mesh module, are time-dependent values and also as the stationary study does not compute these instantaneous velocities. In the study, the time range was selected from 0 s to 1 s with a step of 0.1 s. The applied voltages were limited to 140 V in positive polarization direction and −40 V in negative polarization direction to avoid piezo saturation and re-polarization [8]. A sinusoidal voltage within the voltage limits was defined using a piecewise function under global definitions. Figure 7 a and b show the line plot of voltages applied to the piezoelectric electrodes and also show the membrane deformation.

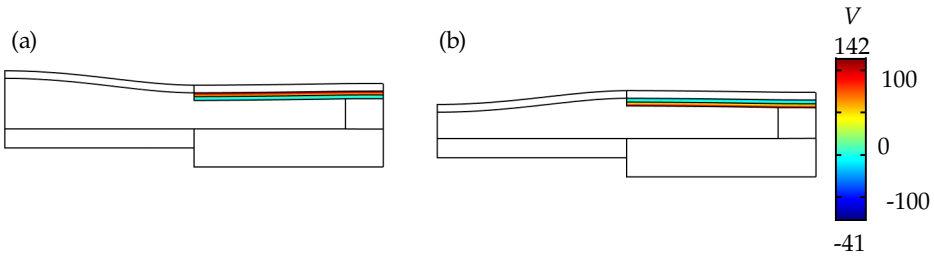

Figure 7. Applied voltages on the piezoelectric actuator with (a) convex lens mode and (b) concave lens mode.

The volume plot in Figure 8 a and b generated by the 2D revolution around the symmetric axis show the adaptive lens in plano-convex and plano-concave lens modes. The revolved plot is used to visualize the aspherical deformation of the membrane. The surface plot in Figure 9 a and b show the membrane deformation and the dynamic internal fluid pressure with the fluid velocity direction for both the applied voltage directions.

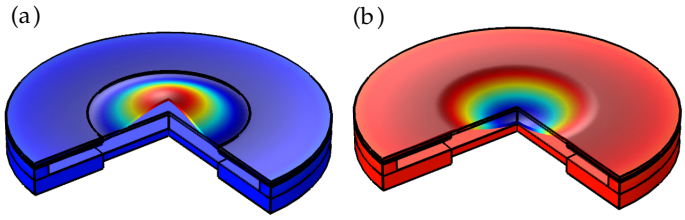

Figure 8. The 2D revolved plots showing (a) aspheric convex lens and (b) aspheric concave lens mode.

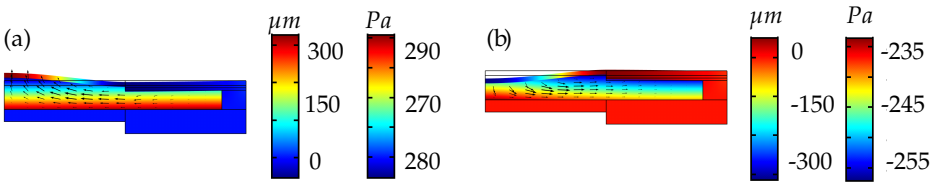

Figure 9. The surface simulation plots of the adaptive lens showing dynamic internal chamber pressure and solid deformation in (a) plano-convex and (b) plano-concave modes.

The heat transfer interface for solids and fluids were used to set the temperatures from 20 °C to 80 °C. The simulation models the membrane deformation due to thermal expansion of the fluid. The surface plot in Figure 10 shows the temperature distribution of the adaptive lens set to 80 °C.

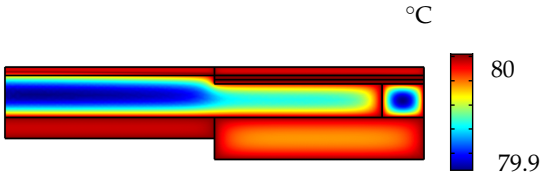

Figure 10. Temperature distribution of the adaptive lens at 80 °C .

The refractive power of the adaptive lens in simulation (Figure 11) was calculated by double differentiation of the membrane boundary with respect to the deformation component (w) and the radial component (r) (Eq 9).

$$Refractivepower = dtang(dtang(w,r,r) \cdot (n-1) \tag{9}$$

where 'w' is the deflection component, 'r' is the radial component and 'n' is the refractive index of the adaptive lens.

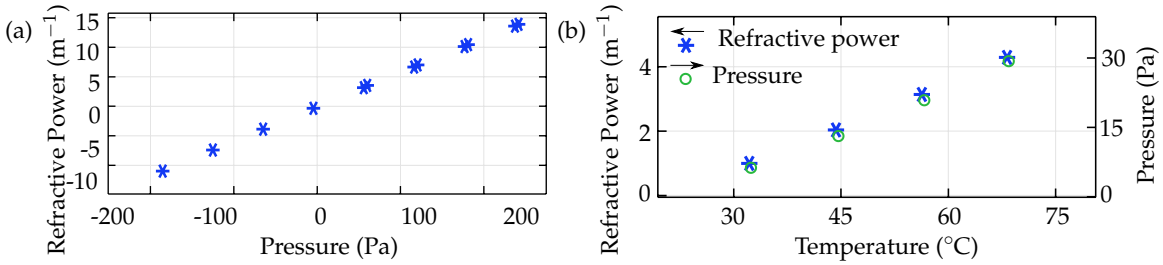

Figure 11. (a)The simulated refractive power of the adaptive lens as a function of fluid chamber pressure, and (b)the change in refractive power of the adaptive lens due to thermal expansion of the fluid.

5. Experiment

Furthermore, to verify the simulation results, we characterized the adaptive lens at different applied voltages and temperatures [7]. The adaptive lens integrated with a pressure sensor and a temperature sensor, to compensate for the non-linear piezoelectric hysteresis and the fluid thermal expansion effect [7], [9], was used in the characterization. The piezoelectric actuator was applied with a sinusoidal voltage like the simulation, and the membrane deformation was measured using a profilometer while simultaneously measuring the pressure sensor and temperature sensor outputs. The refractive power was calculated from the measured membrane surface and was defined as a function of both the internal fluid pressure and the temperature. The simulated and experimented refractive power of the adaptive lens at 25 °C, 50 °C and 75 °C with different applied voltages are compared in Figure 12. The temperature drift of the refractive power in the positive direction is higher than that in the negative direction because of the superposing effects of the thermal expansion of the fluid and the increased actuator deflections at higher temperatures [7], [8].

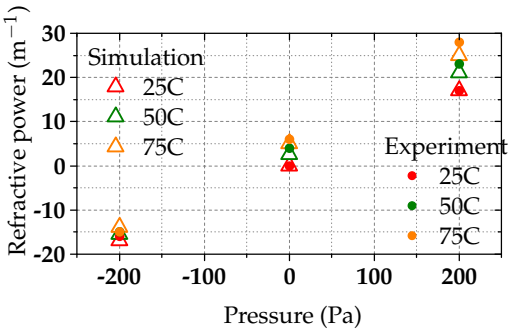

Figure 12. Comparison of the experimented and simulated results of refractive power.

6. Conclusion

The simulation model successfully couples the piezoelectric physics with the laminar flow physics. The adaptive lens was simulated at different voltages and temperatures to determine the actuator deflection, the fluid pressure, and the refractive power. The simulated results are in close agreement with the experimental results. The adaptive lens can vary the refractive power from $-16\,\mathrm{m}^{-1}$ to $17\,\mathrm{m}^{-1}$ at 25 °C and from $-15\,\mathrm{m}^{-1}$ to $28\,\mathrm{m}^{-1}$ at 75 °C. Furthermore, the simulation model could be extended to also model the piezoelectric hysteresis and change in piezoelectric coefficients with the temperature.

Funding: This work was financed by the Baden-Württemberg Stiftung gGmbH under the project VISIR^2 (Variable Intelligent Sensors, Integrated and Robust for Visible and IR light). The article processing charge was funded by the German Research Foundation (DFG) and the University of Freiburg in the funding program Open Access Publishing.

Conflicts of Interest: The authors declare no conflict of interest.

Abbreviations

The following abbreviations are used in this manuscript:

PDMS	Polydimethylsiloxane
FSI	Fluid-structure interaction
FEM	Finite element method
dtang	Differentiation
CNC	Computer numerical control

References

1. Beckers, J.M. Adaptive Optics for Astronomy: Principles, Performance, and Applications. *Annual Review of Astronomy and Astrophysics* **1993**, *31*, 13–62. doi:10.1146/annurev.astro.31.1.13.
2. Booth, M.J. Adaptive optics in microscopy. *Philosophical Transactions of the Royal Society A: Mathematical, Physical and Engineering Sciences* **2007**, *365*, 2829–2843. doi:10.1098/rsta.2007.0013.
3. Weyrauch, T.; Vorontsov, M.A.; Gowens, J.; Bifano, T.G. Fiber coupling with adaptive optics for free-space optical communication. 2002, pp. 177–184. doi:10.1117/12.453227.
4. Schneider, F.; Draheim, J.; Kamberger, R.; Waibel, P.; Wallrabe, U. Optical characterization of adaptive fluidic silicone-membrane lenses. *Optics Express* **2009**, *17*, 11813. doi:10.1364/OE.17.011813.
5. Draheim, J.; Schneider, F.; Kamberger, R.; Mueller, C.; Wallrabe, U. Fabrication of a fluidic membrane lens system. *Journal of Micromechanics and Microengineering* **2009**, *19*, 095013. doi:10.1088/0960-1317/19/9/095013.
6. Uchino, K. *Advanced piezoelectric materials: Science and technology*; 2010; pp. 1–678. doi:10.1533/9781845699758.
7. Gowda, H.G.B.; Wallrabe, U. Integrated Sensor System to Control the Temperature Effects and the Hysteresis on Adaptive Fluid-membrane Piezoelectric lenses. Accepted by International Symposium on Optomechatronic Technologies (ISOT 2019), Goa, India, 2019.

8. Bruno, B.P.; Fahmy, A.R.; Stürmer, M.; Wallrabe, U.; Wapler, M.C. Properties of piezoceramic materials in high electric field actuator applications. *Smart Materials and Structures* **2019**, *28*, 015029. doi:10.1088/1361-665X/aae8fb.
9. Draheim, J.; Burger, T.; Kamberger, R.; Wallrabe, U. Closed-loop pressure control of an adaptive single chamber membrane lens with integrated actuation. 16th International Conference on Optical MEMS and Nanophotonics. IEEE, 2011, pp. 47–48. doi:10.1109/OMEMS.2011.6031036.